Japanese Journal of Applied Physics **50** (2011) 091102 **REGULAR PAPER**
DOI: 10.1143/JJAP.50.091102

Crystalline In–Ga–Zn–O Density of States and Energy Band Structure Calculation Using Density Function Theory

Charlene Chen[1], Kai-Chen Cheng[1], Evgeniy Chagarov[2], and Jerzy Kanicki[1,3*]

[1]*Solid State Electronics Laboratory, Department of Electrical Engineering and Computer Science, University of Michigan, Ann Arbor, MI 48109, U.S.A.*
[2]*Department of Chemistry and Biochemistry, University of California, San Diego, La Jolla, CA 92093, U.S.A.*
[3]*Institute for Telecommunication and Information Technology, University of California, San Diego, La Jolla, CA 92093, U.S.A.*

Received March 9, 2011; revised July 5, 2011; accepted July 9, 2011; published online September 20, 2011

The density of states (DOS) and energy band structure of crystalline In–Ga–Zn–O (c-IGZO) and the impact of point defects on its electronic structure are investigated by first-principles calculations based on the density function theory. The calculated DOS showed that the p-orbitals of the oxygen atoms mostly contribute to the valance band maximum (VBM) of c-IGZO. The conduction band minimum (CBM) is dominated by s-orbitals of the Zn/Ga mixture atoms, while the In atoms have the largest spatial spread of wave function. Oxygen vacancies create fully occupied defect states within the band gap and serve as deep donors. Both hydrogen substitutions and interstitials act like shallow donors, and raise the Fermi level above the CBM. Oxygen split interstitials created fully occupied defect states above VBM, while oxygen octahedral interstitials create both occupied and unoccupied states, and may serve as acceptors.

1. Introduction

Despite the rapid progress in developing a high performance metal oxide semiconductors for flat panel displays, the underlying physics that determine the materials' electrical properties remain mostly unclear. Theoretical simulation of this relatively new class of semiconductor would be beneficial for fundamental understanding and future material design. In 1995 Kimizuka *et al.*[1)] using X-ray diffraction and a high resolution electron microscopy has established that crystalline $InGaZnO_4$ (c-IGZO) compound has layered composition of one $InO_{1.5}$ layer, one $(In,Zn)O_{2.5}$ layer and $(m-1)ZnO$ layers. Nespolo *et al.*[2)] synthesized a single crystal of $InGaZnO_4$, in which In is octahedrally coordinated and Zn/Ga are in trigonal bipyramids. Using X-ray diffraction they found that $InGaZnO_4$ is isotypic with $YbFe_2O_4$ and is built by stacking of oxygen along *c*-axis with a closest packing topology. In (substituting Yb^{3+}) is located between two oxygen planes, in octahedral coordination, whereas Zn^{2+}/Ga^{3+} (substituting Fe^{2+}/Fe^{3+}) are almost on the same plane as the oxygens, in trigonal bipyramidal coordination. Keller *et al.*[3,4)] found that, using X-ray diffraction and bond valance calculations, $InGaZnO_4$ belongs to compounds with general formula $ARO_3(ZnO)_m$ (A, R: trivalent metal ion, *m*: integer). The data show clearly an ordering of the R cation being Ga^{3+}, which occupies the inversion boundary in the wurtzite type region. In^{3+} occupies octahedral sites, which are connected by sharing edges and forming a layer structure parallel to the base plane. The octahedrons have the composition $[InO_2]^-$ and are slightly compressed in the direction of the *c*-axis. This yields O–In–O bond angles, which deviate by 10° from the ideal 90° angle. At both sides, the $[InO_{6/3}^-]_2^-$ layers are connected by corners with ZnO_4 tetrahedra. As results of this structure motif Zn^{2+} changes the site occupation from T^+ to T^- (inversion of the wurtzite structure). The inversion plane is built by Ga^{3+} ions filling trigonal bipyramidal sites in the wurtzite type block at half distance between the layers of InO_6 octahedra. The inversion of wurzite-type domain implies a cubic stacking of close packed layers of oxygen atoms in the region where octahederal sites are occupied by indium. The Zn^{2+} has a slightly distorted tetrahedral co-ordination. Since Zn^{2+} and Ga^{3+} are isoelectric they are indistinguishable by X-ray diffraction. The calculation of the bond valence sum was reasonable only with Zn in tetrahedral sites and Ga in trigonal bipyramidal interstices. Therefore, it is proposed that these compounds crystallize in the rhombohedral space group R3m for m = odd and $P6_3/mmc$ for m = even, respectively.[5)]

In the past few years, several calculations of the electronic structure of crystalline or/and amorphous In–Ga–Zn–O (a-IGZO) based on density function theory (DFT) have been reported. Orita *et al.*[6)] stated that the conduction band minimum (CBM) of c-IGZO is formed by the overlapping of In 5s orbitals, and the InO_2 layers serve as the conduction path. Authors also predicted that a very high conductivity can be achieved if dopant ions are introduced into the $GaZnO_2$ layers, with a negligible scattering carriers effect in the InO_2 layers. Nomura *et al.*[7)] studied the local structure of a-IGZO and reported that the nearest neighbor distances are similar to those in c-IGZO, and the coordination numbers of the ions are reduced in comparison to the crystalline phase, resulting in a smaller bulk density. They also reported, in agreement with Orita, that the CBM is formed by the In 5s orbitals. Medvedeva *et al.*[8)] found that the CBM of c-IGZO is formed by the s-orbitals of all cations and the p-orbitals of oxygen atoms; and the isotropic electron effective mass can be obtained by averaging over those of the corresponding single-cation oxide constituents. Kamiya *et al.*[9,10)] studied the oxygen deficiencies in a-IGZO, and reported that an oxygen defect may serve as an electron trap or a shallow donor depending on its local structure. Omura *et al.*[11)] studied the effect of native point defects in c-IGZO, and suggested that interstitial hydrogen serve as shallow donors, and interstitial oxygen occupying an octahedral interstitial site form defect states that trap both electrons and holes.

In this work, we perform first-principles quantum mechanics calculations of c-IGZO with layered ordered crystalline structure. Electronic structure of c-IGZO is explored through simulation of the band structure and density of states (DOS). The influence of point defects (oxygen vacancies, substitution hydrogen, interstitial hydrogen and oxygen) on c-IGZO the electronic structure is investigated, and compared with the first-principles calculations reported previously for c-IGZO.

*E-mail address: kanicki@umich.edu

2. First-Principles Calculations, Crystalline, and Electronic Structure of c-IGZO

In this study, first-principle calculations were carried out using the CASTEP code[12] based on the DFT plane-wave pseudopotential method[13,14] with the Perdew–Wang generalized-gradient approximation functional (PW91).[15] We used the ultrasoft pseudopotentials[16] which treated the Zn/Ga 3d and In 4d states as valence electrons. A plane-wave basis cutoff energy of 380 eV with a $5 \times 5 \times 2$ k-point grid was employed (spin unpolarized), and the Pulay density mixing scheme[17] was chosen for electronic structure minimization method.

Briefly CASTEP first-principles simulations employ density functional theory to solve single-electron Schrödinger wave equations in a potential $V(\mathbf{r})$

$$\hat{H}\psi_n(\mathbf{r})\left[-\frac{\hbar^2}{2m}\nabla^2 + V(\mathbf{r})\right]\psi_n(\mathbf{r}) = \epsilon_i\psi_n(\mathbf{r}), \tag{1}$$

where $\hat{H}$ is the single-electron Hamiltonian, ϵ_i are the energy eigenvalues, $\psi_n(\mathbf{r})$ are the wavefunctions, and $\mathbf{r}$ is the position vector. Solving the Schrödinger wave equation, the ground-state energy, E_g, of the material of interest can be calculated. With respect to $\mathbf{r}$, the ground-state energy is a function of the electron density, $\rho(\mathbf{r})$, external potentials $v(\mathbf{r})$, and the ground-state expectation value of Hamiltonian H_0, $F[\rho(\mathbf{r})]$, such that

$$E_g < \int d\mathbf{r}\, v(\mathbf{r})\rho(\mathbf{r}) + F[\rho(\mathbf{r})]. \tag{2}$$

The Kohn–Sham equations[14] related the electron density to wavefunctions of non-interacting electrons by

$$\rho(\mathbf{r}) = \sum_{n=1}^{N} \psi_n^*(\mathbf{r})\psi_n(\mathbf{r}) \tag{3}$$

and $F[\rho(\mathbf{r})]$ is written as

$$F[\rho(\mathbf{r})] = E_k[\rho(\mathbf{r})] + E_H[\rho(\mathbf{r})] + E_{xc}[\rho(\mathbf{r})], \tag{4}$$

where E_k is the kinetic energy for the system of non-interacting electrons that produce $\rho(\mathbf{r})$, E_H is the Hartree–Coulomb energy, and E_{xc} is the exchange–correlation energy. The effective potential in the Kohn–Sham methodology is then given by

$$V_{KS}(\rho(\mathbf{r})) = \frac{\delta}{\delta\rho(\mathbf{r})}(E_H[\rho(\mathbf{r})]) = V_H(\rho(\mathbf{r})) + \frac{\delta E_{xc}[\rho(\mathbf{r})]}{\delta\rho(\mathbf{r})}. \tag{5}$$

To closely approximate a solution to the Kohn–Sham equations, the exchange–correlation energy, E_{xc}, is introduced in the form described in the local-density approximation (LDA):

$$E_{xc}[\rho(\mathbf{r})] = \int d\mathbf{r}\, \rho(\mathbf{r})\, \epsilon_{xc}[\rho(\mathbf{r})], \tag{6}$$

where ϵ_{xc} is the exchange–correlation energy per electron. The LDA model assumes that for an infinitesimal density $\rho(\mathbf{r})d\mathbf{r}$, E_{xc} is the same as for a uniform electron gas having a density ρ. While LDA mistakenly assumes a uniform charge density around an atom, the model is found to be reasonably accurate for c-IGZO. Modern forms of the LDA are based on the total energy of the homogeneous electron gas derived from quantum Monte-Carlo calculations.

Following the methodology set forth by Car and Parrinello,[18] CASTEP implements Bloch's theorem to find the wavefunctions of the electrons in the three-dimensional, periodic system of interest. These wavefunction are given by

$$\psi_{n,\mathbf{k}}(\mathbf{r}) = u_{n,\mathbf{k}}(\mathbf{r})\exp(i\mathbf{k}\cdot r), \tag{7}$$

where $u(\mathbf{r})$ is a function having periodicity equal to that of the cell it represents, and in this case represents a series expansion of the plane waves, allowing a series representation of $\psi_{n,\mathbf{k}}(\mathbf{r})$ given by

$$\psi_{n,\mathbf{k}}(\mathbf{r}) = \sum_G u_{n,\mathbf{k}}(\mathbf{G})\exp[i(\mathbf{k}+\mathbf{G})\cdot r], \tag{8}$$

in which case $u_{n,\mathbf{k}}$ are expansion coefficients, $\mathbf{G}$ is the wavevector representative of the unit cell, and the exponential term is representative of the entire system, and not simply the periodic unit cell. Ideally, a system would be made infinite, making a solution to $\psi_{n,\mathbf{k}}(\mathbf{r})$ tractable, but computationally is inefficient. If, however, $\mathbf{k}$ is sampled at points close enough together, variation of $\psi_{n,\mathbf{k}}$ with $\mathbf{k}$ becomes negligible and computational expense is saved. The set of wavevectors $\{\mathbf{G}\}$ also ideally would be infinite to achieve an exact solution, but this as well is neither necessary nor computationally worthwhile to achieve an accurate solution. Furthermore, $\{\mathbf{G}\}$ is typically chosen to cover a grid representing the reciprocal space of the system, and along with $\mathbf{k}$, is used to determine a cutoff for the number of plane-waves required by the computation. Simply put, the energy of a free electron whose wavefunction has the same wavevector as the largest wavevector in the plane-wave basis set determines a cutoff energy

$$E_c = \frac{\hbar(\mathbf{G}+\mathbf{k})^2}{2m}, \tag{9}$$

where m is the electron mass. Thus only plane-waves having energy less than E_c are used in the series expansion in eq. (8).

Many assumptions are made during CASTEP quantum mechanical calculations that do not exactly correlate to real world condition. Primarily, calculation are assumed to be performed a 0 K and in vacuum. Thus, the effects of pressure and temperature are not included in these calculations; CASTEP does have ability to do dynamic calculations with variable pressure and temperature.

In this work, the electronic properties were calculated using the local density approximation (LDA) method; the generalized gradient approximation (GGA) gave similar results. The GGA introduces a dependence of exchange–correlation functional on the local gradient of the electron density. A plane-wave based cutoff of $E_c = 10.0$ eV, with norm-conserving pseudo-potentials, was used. Gaussian smearing functions of 0.1 eV were applied to the electronic bands to attain the density of states. Parameters used here for CASTEP density of states (DOS) and energy band structure calculation are outlined in Table I.

It is also worth noting that models such as LDA and GGA under-calculate the energy bandgap, necessitating the application of a scissors operator to shift the conduction band to match experimentally obtained bandgaps. In this work, scissors operators are applied when needed. Following eqs. (1)–(6), the energy eigenvalues are known in k-space,

Table I. Example of settings for CASTEP first principles calculations.

Setting	Value
Plane-wave basis cutoff	10.0 eV
Pseudopotential	Ultrasoft
Exchange correlation	GGA
Scissor operator	1.59 eV
DOS smearing	0.1 eV

and so as energy structure can be determined for c-IGZO. Gaussian smearing width of 0.1 and 0.2 eV were applied to the orbital occupancy and total DOS simulation, respectively. The total DOS represent the sum of s-, p-, and d-orbital for In, Ga, Zn, and O.

As a reference, first principles calculation were performed on intrinsic crystalline silicon (c-Si) to ensure simulation results are reasonable. The electronic bandstructure of c-Si is well known, both experimentally and theoretically, being, for example, an indirect bandgap semiconductor with an energy bandgap of 1.1 eV. The calculated bandstructure of c-Si is shown that the energy bandgap is readily observed to be indirect, with $E_G = 1.1$ eV after applying a Gaussian smear function of 0.5 eV. In the valence band, light-hole, heavy-hole, and split-off bands are observed. The DOS of c-Si indicates the formation of wide allowed bands.

In the present work we used the layered ordered crystalline structure of In–Ga–Zn–O[6] (shown in Fig. 1) that adopts rhombohedral symmetry (space group: $R\bar{3}m$ when m is an odd number) with lattice parameters $a = b = 3.295$ Å, $c = 26.07$ Å, $\alpha = \beta = 90°$, and $\gamma = 120°$. Layered structure has alternating laminated layers of one layer of InO_2^- interlaced with two layers of $GaO(ZnO)^+$ along c-axis. These layers accumulate to form a unit cell in the following order: InO_2^-, $GaO(ZnO)^+$, $GaO(ZnO)^+$, InO_2^-, $GaO(ZnO)^+$, $GaO(ZnO)^+$, InO_2^-, $GaO(ZnO)^+$, and $GaO(ZnO)^+$; e.g., we could also say that n pieces of $(GaZn_m)O_m^+$ layers contain m pieces of ZnO layers. The In^{3+} ions in the InO_2^- layer form InO_6 octahedra, which are two-dimensionally connected in an edge-sharing network. Since no extra diffraction spots were found in X-ray diffraction pattern, the Ga^{3+} and Zn^{2+} ions are randomly distributed at 6c crystallographic positions between InO_2^- layers; they occupy the trigonal–bipyramidal sites (MO_5) in the $GaO(ZnO)^+$ layers, and are each coordinated by five oxygen atoms. To reflect Ga/Zn atoms random distribution within $GaZnO_2^+$ layers we adopted in this calculation "mixture atoms" or "random atoms" approach by using a composition of 50% Ga and 50% Zn within each $GaZnO_2^+$ layer. The bond lengths and bond angles between metal and oxygen atoms of InO_6 and MO_5 are illustrated in Fig. 2. The crystal data for c-IGZO used in this calculation is summarized in Table II.

Although the Zn^{2+} and Ga^{3+} are isoelectric and thus indistinguishable by X-ray diffraction (e.g., no extra diffraction spots are found), the structure refinement based on a model with different z coordinates for Ga and Zn can still give a good fit to the observed diffraction pattern. The change in the atomic position had some effect on the electronic structure mainly through changes in the Madelung potential. A geometry optimization calculation was then performed on the initial unit cell using the Broyden–

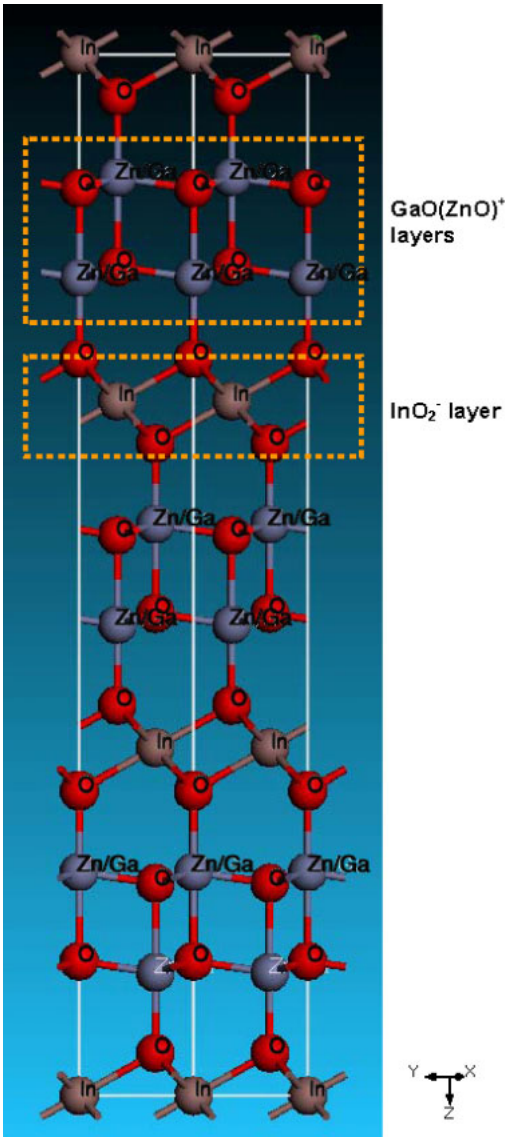

Fig. 1. (Color online) Crystalline structure of In–Ga–Zn–O used in this work.

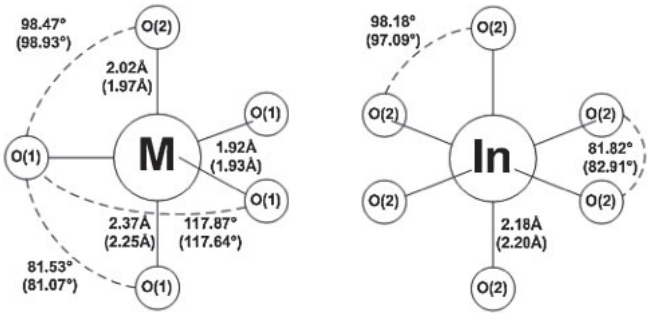

Fig. 2. Bond lengths and bond angles of MO_5 and InO_6 in c-IGZO used in this work. Values inside the parentheses are of the relaxed structure after geometry optimization. Experimental values are given in Table II for reference.

Fletcher–Goldfarb–Shanno (BFGS) algorithm.[19] The cell size and the coordinates of the atoms were adjusted by an iterative process so that the total energy of the structure is minimized. The convergence criteria for the geometry

Table II. Crystalline structure of $InGaZnO_4$[6,37] with values inside the parentheses of the relaxed structure after geometry optimization. Crystal data and refinement results for $GaInZn_4O_7$ are also given in ref. 38. Experimental data shown in this table were taken from ref. 28.

Space group	$R\bar{3}m$		Exp.
Lattice parameters in hexagonal axes	$a = b = 3.29$ (3.37) Å, $c = 26.07$ (26.19) Å $\alpha = \beta = 90°$, $\gamma = 120°$		$a = b = 3.2990$ Å $c = 26.101$ Å
Anisotropic displacement parameters	In (0, 0, 0)	[(0, 0, 0)]	(0, 0, 0)
	Ga/Zn (0, 0, 0.21)	[(0, 0, 0.22)]	(0, 0, 0.2171)
	O(1) (0, 0, 0.13)	[(0, 0, 0.13)]	(0, 0, 0.1282)
	O(2) (0, 0, 0.29)	[(0, 0, 0.29)]	(0, 0, 0.2928)
Bond lengths (Å)	In–O(2)	2.18 (2.23)	2.1784
	M1–O(1)	1.92 (1.97)	1.9302
	M1–O(2)	2.02 (2.00)	1.977
	M1–O(1)	2.37 (2.25)	2.319
Bond angles (°)	O(2)–In–O(2)	98.18 (97.99)	98.43
	O(2)–In–O(2)	81.82 (82.01)	81.57
	O(1)–M1–O(1)	117.87 (117.84)	117.43
	O(1)–M1–O(2)	98.47 (98.52)	99.32
	O(1)–M1–O(1)	81.53 (81.48)	80.68

optimization were: total energy $= 5.0 \times 10^{-6}$ eV/atom, force $= 0.01$ eV/Å, stress $= 0.02$ GPa, and displacement $= 5.0 \times 10^{-4}$ Å. The calculated data used for this optimization (not shown in this paper) can be well described by Birch–Murnaghan equation of state.[20] The relaxed bond lengths and bond angles are listed in the parentheses in Table II and Fig. 2. The relaxed structure is very close (within 3%) to that determined by single crystal X-ray diffraction measurements.[21]

Figure 3 shows the calculated band structure and total DOS profile. All energies are relative to the Fermi level (shifted to 0 eV). Band structures along the high symmetry k-points in the Brillouin zone, $\Gamma(0, 0, 0)$, $A(0, 0, 1/2)$, $H(-1/3, 2/3, 1/2)$, $K(-1/3, 2/3, 0)$, $M(0, 1/2, 0)$, $L(0, 1/2, 1/2)$, are displayed. The valence band maximum (VBM) is observed to be dispersionless (nearly flat) compared to the conduction band minimum (CBM). The band gap located at the Γ-point is substantially underestimated (1.47 eV) compared to the experimental value (3.05 eV),[22] which is a well known problem of DFT calculations based on the LDA and GGA functionals.[23] LDA is believed to accurately describe the total energy of pure semiconductors. However, the LDA underestimates the fundamental band-gap energies, the optical transition energies, of semiconductors by more than 50%, which in general affects the calculation of defect formation energy. For intrinsic semiconductors, the LDA band-gap error is not a problem since the total ground state energy does not depends on the conduction band energy states. However, the theoretically derived defect energies could possess large uncertainties due to the inaccurate description of the band structure in using the local density functionals and exceedingly slow energy convergence with the supercell size.[24,25] The calculation methods such as hybrid functionals, the Heyd–Scuseria–Ernzerhof (HSE) functional, GW or "postprocessor" corrections applied after DFT energies were calculated, can be used for accurate calculation of the gap that is consistent with the experimental value. It was also established for ZnO that different methods

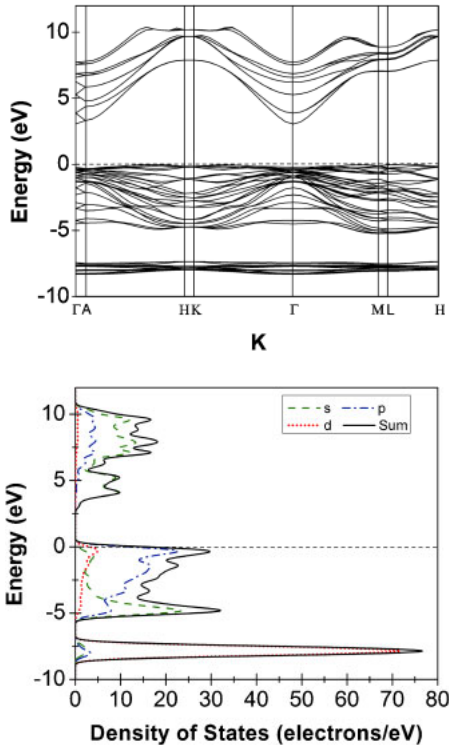

Fig. 3. (Color online) Calculated energy band structure and total density of states of c-IGZO (Fermi level: 0 eV). The 0 eV point represent the top of the respective occupied states.

give remarkably uniform results for the formation energies of the charge-neutral lattice vacancies such as oxygen vacancy.[26] For a number of calculations (unit, super cells and oxygen vacancies) shown in this work scissors operator has been applied (this is one of the feature of Materials Studio software) to match the calculated energy band-gap with the experimental value measured for our films.

The total DOS shown in Fig. 3 are broken down into the s-, p-, d-states. Examination of the DOS profile indicates that the VBM and CBM are mainly composed of the p- and s-states, respectively. The DOS contributed from each atom can be further observed from Fig. 4. We can see that the VBM is dominated by the two fully-occupied p-orbitals of oxygen atoms, while the CBM is mainly formed by the empty s-orbitals of the Ga/Zn mixture atoms. Although contribution to p-orbital of the oxygen atom can be observe to conduction bands. The Ga and Zn atoms are intermixed in the same layer and separated from the In-driven bands.

The spatial distribution of ions s orbitals can be investigated using contour maps. Figure 5 shows the iso-surface of wave functions $|\psi_n|^2$ of conduction band minimums (CBMs) ("Reverse rainbow" is used in this figure to map given color to its value. Red means high and blue means low.). From DOS, we can see that Zn/Ga contributes to more low energy CBM states. But the In 5s orbitals have the largest spatial spread of wave function, and are nearly overlapping with the neighboring orbitals that can create a continuous conduction carrier path. Hence, our result shown in Figs. 4 and 5 mostly agrees with Omura *et al.*'s[11] observation: Ga (in our case, Ga/Zn mixture atom) s-states contribute most to the CBM, while the In s-states have the largest spatial spread of the wave function. It

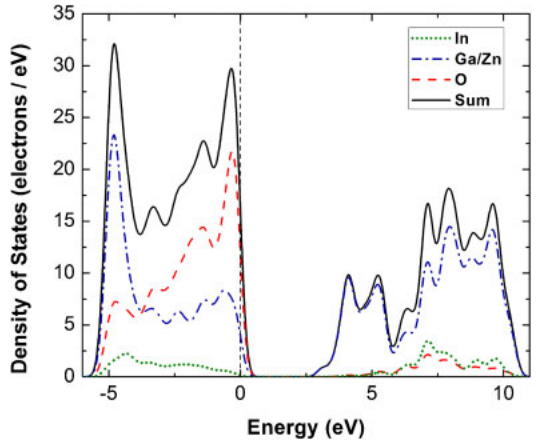

Fig. 4. (Color online) The density of states contributed by each atom, In, Ga/Zn, and O (Fermi level: 0 eV). The 0 eV points represent the top of the respective valence band.

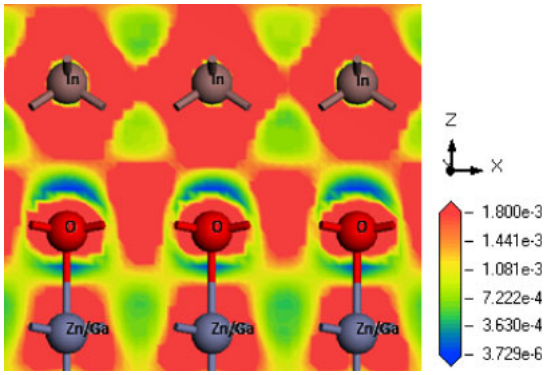

Fig. 5. (Color online) Orbital drawing of the conduction band minimum (color mapping: reverse rainbow).

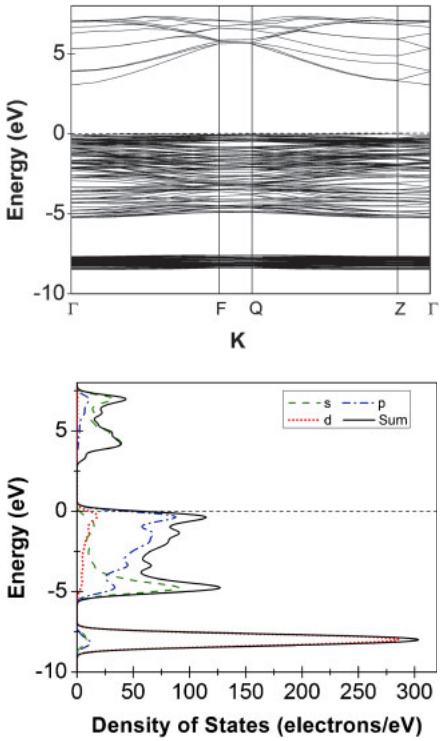

Fig. 6. (Color online) Band structure and total density of states of c-IGZO supercell (Fermi level: 0 eV). The 0 eV points represent the top of the respective valence bands.

should be noticed that since the valence state and ionic radii of Ga and Zn are different, the positions of these atoms is expected to be different. The local structure Rietveld refinement show that the z coordinates of the Ga and Zn sites differ by 3 to 4%. The random displacement of the Ga and Zn atoms causes small overlapping of the 4s orbital of Ga and/or Zn, which is in agreement with the simulation results shown in Fig. 5. This will lead to the insulating nature of the $GaZnO_2$ layer. However due to some overlap between In 5s and Ga 4s orbitals, in spite of the difference in the z coordinates of Ga and Zn, it is expected that the c-IGZO will exhibit a three-dimensional network for electron transport with isotropic effective mass. The neighboring In ions connected by edge-sharing network of (InO_6) octahedral will contribute to reduction of the In–In distances as compared to corner-sharing structures (as known in the crystal chemistry) leading to calculated large overlaps of the In ions s-orbitals.[27] This suggests that the direct overlapping of In 5s orbitals due to In–In bond length reduction should be at the origin of a high electrical conductivity (and carrier mobility) in the c-IGZO layer; the In 5s states are considered to be conduction paths for carrier electrons. It should be notice that the In–In atomic distance in the InO_2^- layer is smaller in comparison to Sn-doped In_2O_3 layer which has a high carrier mobility. In agreement with this calculation, the experimental electron mobility of a-IGZO increases with the fraction of In_2O_3 content, and the incorporation of Ga^{3+} is very effective in suppressing electron carrier generation possibly due to the high ionic potential which is able to tightly attract oxygen ions.[28] It is expected and experimentally observed that the carrier mobility and carrier density will decrease with the increasing Ga^{3+} content in c-IGZO. However, further investigation that separates the effect of Zn^{2+} and Ga^{3+} is needed for better understanding of their role in c-IGZO. Also the direct s-s orbitals overlap is rather insignificant. Hence we could question if s-s orbitals interactions, which are commonly assumed to play critical role in the electronic properties of a-IGZO, are responsible for the transport properties in this material?

3. c-IGZO Super Cell with Point Defects

A supercell structure was used to simulate the effect of point defects on DOS of c-IGZO. The supercell has lattice parameters that are multiples of those of the original unit cell ($2 \times 2 \times 1$). Energy calculation was performed on the defect-free supercell (total of 84 atoms) and similar band structures (band gap: 1.37 and 3.05 eV before and after "postprocessor" correction was applied) and DOS were obtained (Fig. 6) in comparison to those of the original unit cell (Fig. 3). Please note that band structures along different high symmetry k-points: $\Gamma(0,0,0)$, $F(0,1/2,0)$, $Q(0,1/2,1/2)$, $Z(0,0,1/2)$ were displayed because of the P1 symmetry, and higher DOS were obtained due to the larger amount of atoms included in the supercell. The reduction in calculated band gap for supercell value in comparison to value calculated for unit cell is due to Gaussian smearing effect. We have confirmed through simulation when

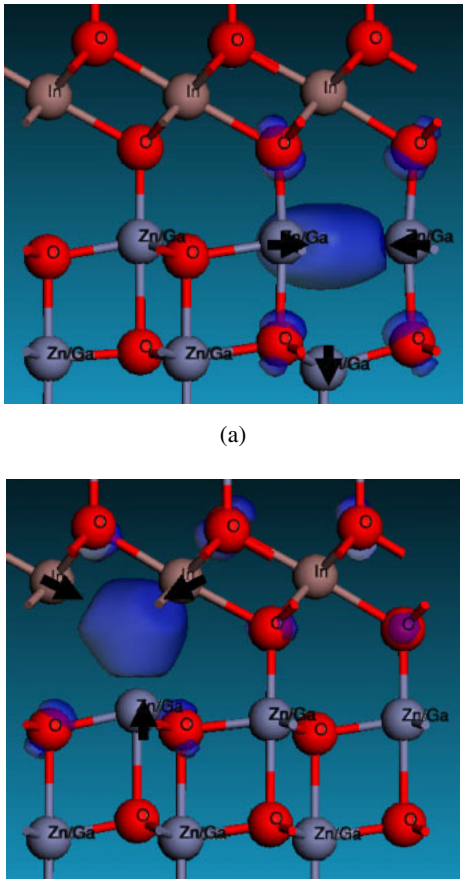

(a)

(b)

Fig. 7. (Color online) Isosurface of the highest occupied band of (a) O_{V1} and (b) O_{V2}.

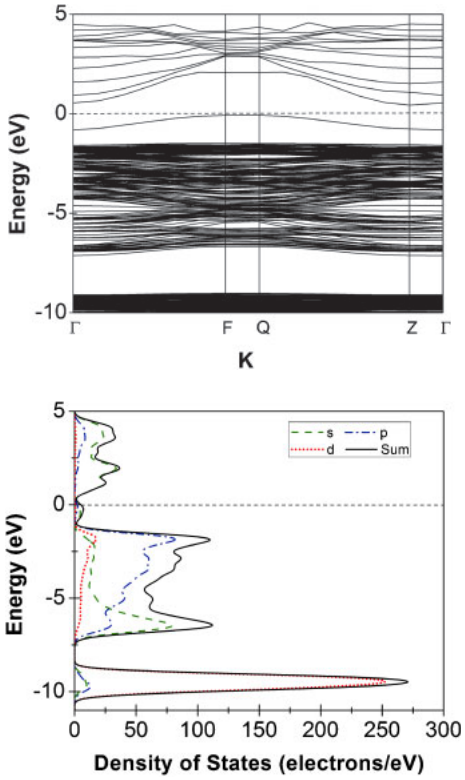

Fig. 8. (Color online) Band structure and total density of states of c-IGZO supercell with oxygen vacancy. The 0 eV points represent the higher occupied states.

smearing value for unit cell is increased the gap is reduced. Hence when we move from unit cell to super cell it is expected (as theoretically simulated) that the band gap is reduced with the increasing number of super cells since the smearing effect is increased with number of super cells.

Several types of point defects were then introduced into the supercell, including oxygen vacancies, hydrogen substitutions, hydrogen and oxygen interstitials, which will be described in more detail in next sub-sections. For all cases, geometry optimization calculation was performed, especially to relax the atoms surrounding the defect (the cell size was kept constant). Then total energy calculation was carried out to study the electronic structures.

3.1 Oxygen vacancies in c-IGZO

Oxygen vacancies (V_o) were created at two different sites. In O_{V1}, an oxygen atom bonded between four Zn/Ga mixture atoms was removed, while in O_{V2}, an oxygen atom bonded between three In and one Zn/Ga mixture atoms was removed. Figures 7(a) and 7(b) shows the relaxed structure of O_{V1} and O_{V2}, respectively. The arrows indicate the displacement vectors of the surrounding atoms after relaxation. In O_{V1}, the three Zn/Ga mixture atoms located in the same $GaO(ZnO)^+$ layer are displaced inward by 8–10% of the equilibrium Zn–O bond length, while the Zn/Ga mixture atom located in the neighboring $GaO(ZnO)^+$ layer is displaced outward by ~5%. In O_{V2}, the three In atoms are displaced inward by 3–5%, and the one Zn/Ga mixture atom is displaced inward by 9%. O_{V1} and O_{V2} have very similar band structure and density of states, Fig. 8. In both cases, oxygen vacancies form fully occupied defect states within the band gap, and raises the Fermi level above the VBM towards the CBM. The isosurfaces (isovalue = 0.04) of the highest occupied bands for O_{V1} and O_{V2} are shown in Fig. 7. It can be seen that the defect state is highly localized around the oxygen vacancy sites for both cases. The physical properties of oxygen vacancies in c-IGZO can be explained based on the electronic structure of oxygen vacancies in ZnO proposed by Janotti and Van de Walle.[29] Following their terminology the removal of an oxygen atom from a perfect c-IGZO leaves four dangling bonds on the surrounding coordinated metal cations, forming a symmetric a_1 state located in the band gap and three higher energy states above the CBM. The a_1 state is fully occupied by two electrons contributed by the four coordinated metal cations each contributing 1/2 electron to a neutral vacancy, and its energy is lowered when the four metal cations approach each other.

The n-type conductivity of a-IGZO has been observed experimentally to vary with the partial pressure of oxygen during the film deposition and/or thermal annealing process.[30] The film resistivity increases (carrier density and mobility decrease) with increasing oxygen partial pressure. So far, oxygen vacancies have been traditionally viewed as the source of unintentional n-type doping of the a-IGZO. However, based on our calculation result (Defect energy value is determined from *E–k* diagram. It is the energy difference between the conduction band minimum (0.44) and the highest energy of the defect (−0.08). We assume that the defect level is located at middle of the defect

states.), oxygen vacancies introduce fully occupied defect states 0.89 eV below the CBM, with defect band width of 0.74 eV. Since the calculated band gap of supercell with oxygen vacancy is 1.93 eV, these defects are deep rather than shallow donor states. Hence they could not create free carriers. Since V_o is fully occupied by electrons it should be considered as inactive site for additional electron trapping. It should be noticed that the calculated DOS are actually discreet values and are all broadened by a Gaussian with a smearing width of 0.2 eV. Because of the band gap underestimation discussed above, it is not possible to provide exact energy location of oxygen vacancies within electronic gap for c-IGZO. However, the conclusion of this simulation is very clear that oxygen vacancies are deep states and their energy position is not be affected by underestimation of the calculated energy gap. When we applied the scissor operation to calculated energy gap, the oxygen vacancies, energy level shifted to ~2.01 eV below CBM (or above 1.09 eV above VBM). Similar conclusion was reached for ZnO.[31)]

3.2 Hydrogen substitutions in c-IGZO

The c-IGZO supercell with a substitutional hydrogen atom located on an oxygen site was also investigated. This configuration can be regarded as a complex consisting of a hydrogen atom and oxygen vacancies. Defects were created at two different sites. In H_{S1}, a hydrogen atom was placed at O_{V1} (bonded between four Ga/Zn mixture atoms), and in H_{S2}, a hydrogen atom was placed at O_{V2} (bonded between three In atoms and one Ga/Zn mixture atoms). Figures 9(a) and 9(b) show the relaxed structure of H_{S1} and H_{S2}, respectively. The arrows indicate the atom displacement directions during the geometry optimization process. We can see that the substitutional hydrogen atom forms a longer bonding with the Zn/Ga mixture atom located in the neighboring $GaO(ZnO)^+$ layer. In H_{S1}, the hydrogen atom and the Zn/Ga mixture atom is displaced outward by ~9 and 6%, respectively, while in H_{S2}, the displacement is ~2 and 11%, respectively. Figure 10 shows the similar band structures and density of states shared by H_{S1} and H_{S2}. We can see that the addition of hydrogen atoms turn the oxygen vacancies into shallow donors, and raises the Fermi level above the CBM, and do not form any in-gap states. The H 1s orbital combines with the a_1 state and results in a bonding state located deep in the valence band, and an antibonding state in the conduction band. Two of the three electrons (one from the hydrogen atom, and two from the coordinating metal cations) occupy the bonding state. The third electron occupies the antibonding state and then relaxes to the CBM. Hence, our calculated c-IGZO electronic structure is in agreement with the proposed electronic structure of hydrogen substitutions occupying oxygen sites in ZnO.[32)] The bonding state is found to be ~6 eV below the VBM and the lowest energy antibonding/nonbonding states are found to be ~1 eV above the CBM [isosurfaces are shown in Figs. 9(a) and 9(b) respectively]. We observe that the six next-nearest-neighbor oxygen atoms contribute to the bonding state orbital, the bonding seems to be weaker to the Zn/Ga mixture atom located in the neighboring $GaO(ZnO)^+$ layer, possibly because of the alternating layered structure.

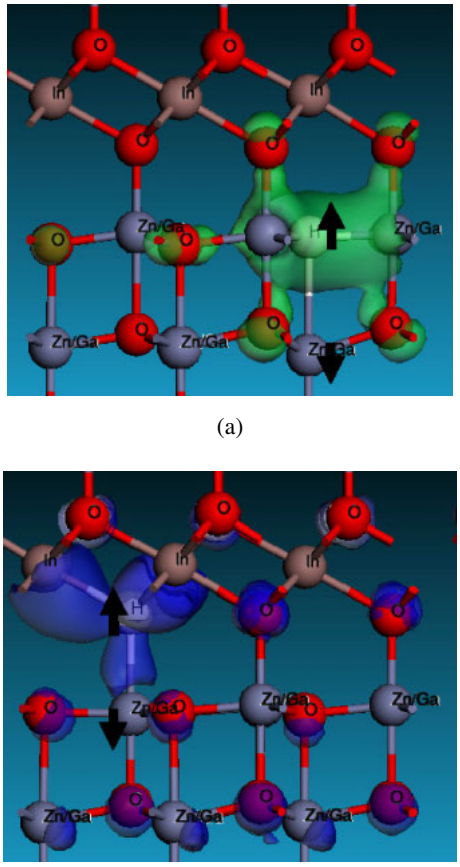

Fig. 9. (Color online) Relaxed structures of (a) H_{S1} and (b) H_{S2}. Isosurfaces of the bonding state (a) and the lowest energy antibonding/nonbonding states (b) are also shown.

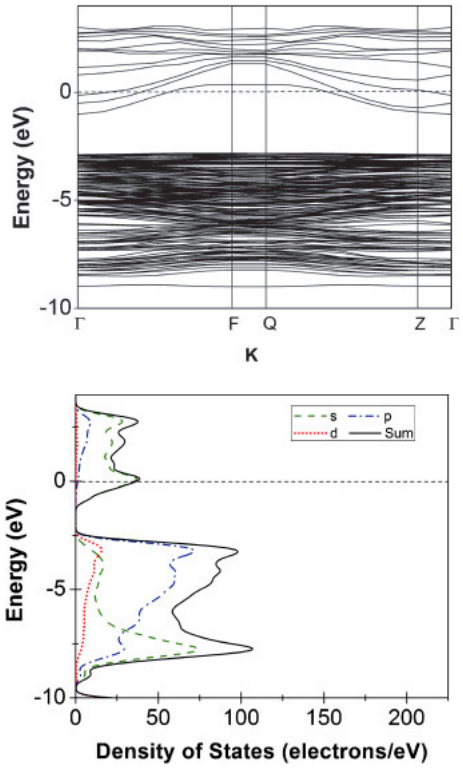

Fig. 10. (Color online) Band structure and total DOS of c-IGZO supercell with hydrogen substitution. The 0 eV points represent the higher occupied states.

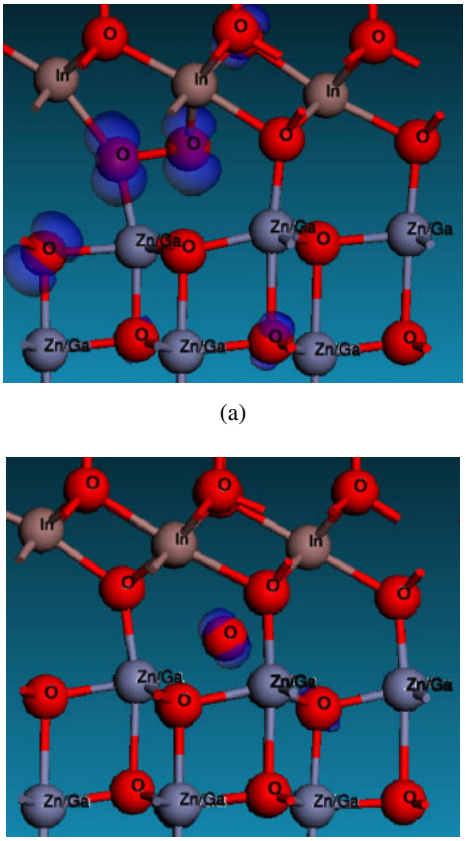

(a)

(b)

Fig. 11. (Color online) Relaxed structures of (a) O_{split} and (b) O_{oct}. Isosurfaces of the oxygen interstitial defect states are also shown.

Therefore, based on our simulation results, the dependency of c-IGZO dark conductivity on oxygen partial pressure could be explained by hydrogen substitutions located on oxygen sites, since hydrogen can be easily incorporated during film growth or/and thermal annealing processes. Experimental results have confirmed presence of hydrogen in a-IGZO[33] and it is shown experimentally that hydrogen is capable to dope a-IGZO[34] and to reduce its dark resistivity.

3.3 Oxygen interstitials in c-IGZO

Two different oxygen interstitial configurations were explored, split (O_{split}) and octahedral (O_{oct}). In O_{split}, the interstitial oxygen atom (O_i) was initially placed at an antibonding site of an In–O bond, 1.46 Å from the oxygen atom (O_o). After geometry optimization [as shown in Fig. 11(a)], the O_i–O_o bond length became 1.51 Å, forming a weaker bond compared to that of an isolated O_2 molecule (1.21 Å). O_i and O_o each bonds to two metal cations, and occupy the same lattice site, forming a split interstitial. The In–O and M–O bonds are shortened by 1–2.5% compare to the defect free structure. In O_{oct}, the interstitial oxygen atom (O_i) was placed at an octahedral site coordinated by six oxygen atoms (O_o). After relaxation, the six surrounding O_o atoms displaced outward from O_i by 8–10% of the unrelaxed interatomic distance [as shown in Fig. 11(b)]. It is reported by other first-principles studies that oxygen interstitials occur at either split or octahedral sites in c-IGZO[11] which agrees with our results.

Figures 12(a) and 12(b) show the simulated band structure and density of states of O_{split} and O_{oct}, respectively. We observed that O_{split} forms fully occupied deep level states

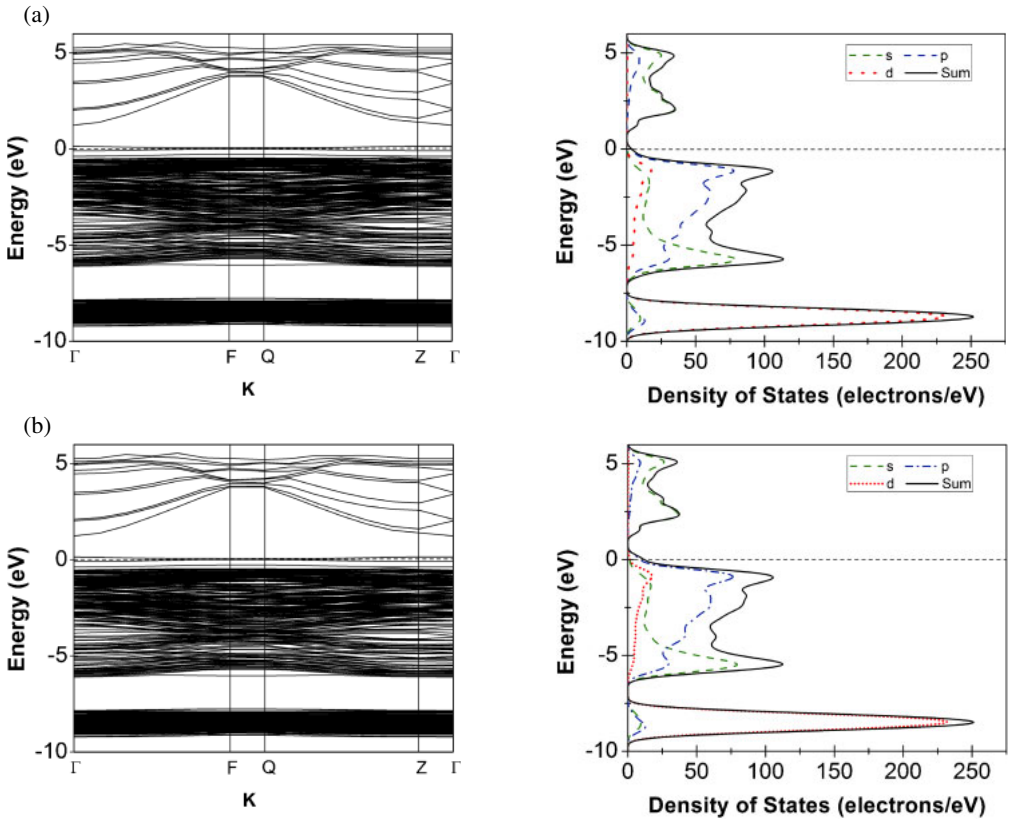

Fig. 12. (Color online) Band structure and total DOS of c-IGZO supercell with oxygen interstitial (a) O_{split} and (b) O_{oct}. The 0 eV points represent the higher occupied states.

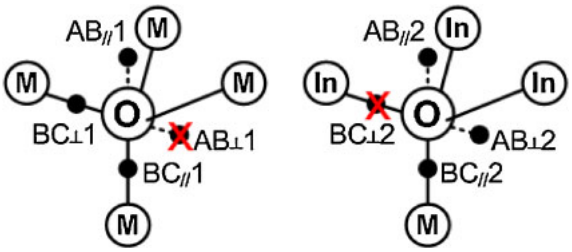

Fig. 13. (Color online) Hydrogen interstitial sites.

above the defect-free valence band maximum (VBM_0). The isosurface of the defect states is shown in Fig. 11(a), which is mainly associated with the O_i–O_o anti-bonding ppπ^* orbital (doublet, only one is shown). Other O_i related localized states were also observed including ssσ at −21 eV, and ssσ^* at −15.5 eV. If we assume that split interstitials formed by first row elements C, N, and O on oxygen sites in ZnO can be described by substitutional diatomic molecules, then the physical property of the O_i–O_o defect is very similar to that of the free O_2 molecule with molecular orbitals ssσ, ssσ^*, ppσ, ppπ (doublet) located in the valence band filled with ten electrons, and ppπ^* (doublet) located slightly above the VBM_0 filled with the remaining two electrons of the O atoms, and two electrons contributed from the four coordinating metal cations. The longer O_i–O_o bond length can also be explained by the addition of extra electrons to the anti-bonding ppπ^* orbitals. By contrast, O_{oct} forms both occupied and unoccupied states above VBM_0. The defect states are mainly contributed by the p-orbitals of O_i [isosurface shown in Fig. 11(b)], and serves as deep acceptors. Our result agrees with other reported first-principles studies for c-IGZO[11] indicating that oxygen interstitials can exist as electrically inactive split interstitials, or as deep acceptors at the octahedral site in n-type semiconductor. Since state O_{split} forms states inside valence band states, the fundamental issue associated with the underestimation of the band gap will have no impact on conclusion of this simulation.

3.4 Hydrogen interstitials in c-IGZO

Hydrogen interstitial atoms were placed at eight different sites, close to an oxygen atom to form an O–H bond, as shown in Fig. 13. BC indicates the bond-center sites, and AB indicates the anti-bonding sites. The symbol "∥" means the O–H bond is parallel to the *c*-axis; other bond directions are denoted by "⊥". The hydrogen atom was initially placed 1 Å from an oxygen atom. After geometry optimization, $H_{AB\perp 1}$ relaxed into $H_{BC\parallel 1}$, and $H_{BC\perp 2}$ relaxed into $H_{AB\perp 2}$, while the other six interstitial sites seem stable. Figure 14 shows the relaxed structure of two examples, $H_{BC\parallel 1}$ and $H_{AB\perp 2}$. In $H_{BC\parallel 1}$, the optimized O–H bond length was 0.974 Å, and the oxygen and Zn/Ga mixture atoms located on the same bond moved outward by ∼11 and 13% of their original M–O bond, respectively. In $H_{AB\perp 2}$, the optimized O–H bond length is 0.985 Å, and the oxygen moved outward by ∼19% from the In atom, while the Zn/Ga mixture atom shifted downward by 14%. All of the six stable hydrogen interstitial models resulted in similar band structures and density of states, as shown in Fig. 15. Comparing to the

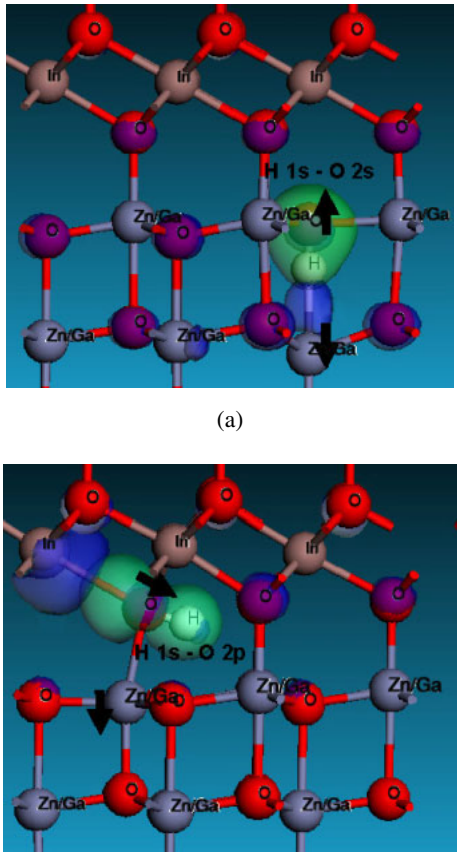

(a)

(b)

Fig. 14. (Color online) Relaxed structures of (a) $H_{BC\parallel 1}$ and (b) $H_{AB\perp 2}$. Isosurfaces of the H 1s–O 2s (a), H 1s–O 2p (b) bonding orbitals, and metal cation dangling bond orbitals are also shown.

defect free c-IGZO supercell (Fig. 6), the main differences are the higher Fermi level located above the CBM and the hydrogen interstitial related states located at energy levels of −22 and −9 eV. The isosurfaces of the localized states around −22 and −9 eV are plotted in Figs. 14(a) and 14(b), and it can be seen that they are associated with the H 1s–O 2s, and H 1s–O 2p bond orbitals, respectively. Hence it can be concluded that the hydrogen interstitial atoms bond strongly to oxygen atoms. Also, from our calculated electronic structure, we have found the metal cation dangling bond state to be ∼1 eV above the CBM (isosurface shown in Fig. 14). Similar electronic structures were previously reported for first-principles calculation of c-IGZO.[11] Therefore it is expected that the neutral oxygen vacancies in combination with the hydrogen could create shallow donor states. The band gap underestimation discussed above will have no impact on the conclusion about the hydrogen substitution and hydrogen interstitial related states since they are located deep inside the conduction band.

4. Conclusion

The first principles simulations were performed for crystalline In–Ga–Zn–O. The calculated electronic structure showed that the valence band maximum (VBM) is mostly composed of the p orbitals of the oxygen atoms. The conduction band minimum (CBM) mainly consists of the

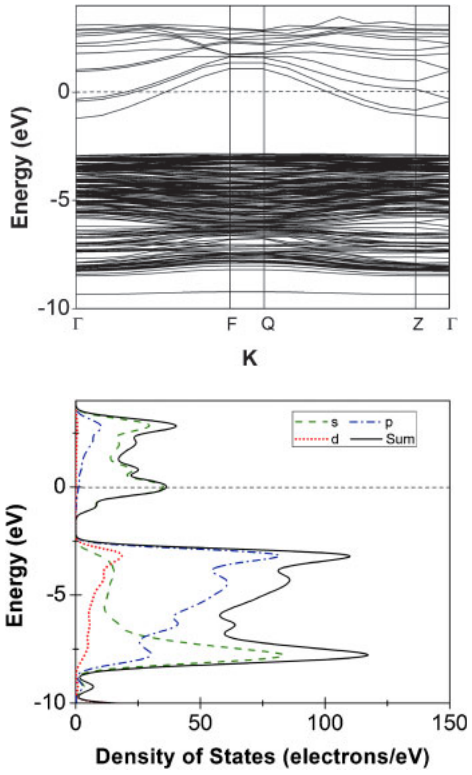

Fig. 15. (Color online) Band structure and total DOS of c-IGZO supercell with hydrogen interstitial. The 0 eV points represent the higher occupied states.

s orbitals of the Zn/Ga atoms mixture, with the In atoms having the largest spatial spread of states corresponding to CBM. The effect of different point defects was also investigated. Oxygen vacancies created fully occupied neutral defect states within the band gap that is electrically inactive. Both hydrogen substitutions (H_s) and interstitials (H_i) act like shallow donors, and raise the Fermi level above the CBM. Oxygen split interstitials created fully occupied defect states above VBM, while oxygen octahedral interstitials create both occupied and unoccupied states, and may serve as deep acceptor states in c-IGZO. Our simulations results of H_s and H_i could theoretically explain the dependence of IGZO dark conductivity on oxygen partial pressure[35] and its behavior when subjected to hydrogen plasma treatment.[36] The hydrogen atoms would act as a donor states in c-IGZO. Also hydrogen interstitial can easily combine with the oxygen vacancies to form a complex that could also behave as a shallow donor.

Acknowledgements

We would like to thank Applied Material Corporation (AKT America Inc.) for supporting this work. One of us (J.K.) would like to thank Dr. Noboru Kimizuka, Dr. M. Orita, and Dr. K. Nomura for very useful discussions and suggestions.

1) N. Kimizuka, M. Isobe, and M. Nakamura: J. Solid State Chem. **116** (1995) 170.
2) N. Nespolo, A. Sato, T. Osawa, and H. Ohashi: Cryst. Res. Technol. **35** (2000) 151.
3) I. Keller, W. Assenmacher, G. Schnakenburg, and W. Mader: Z. Anorg. Allg. Chem. **635** (2009) 2065.
4) I. Keller and W. Mader: Z. Anorg. Allg. Chem. **636** (2010) 1045.
5) M. Isobe, N. Kimizuka, N. Nakamura, and T. Mohri: Acta Crystallogr., Sect. C **50** (1994) 332.
6) M. Orita, H. Tanji, M. Mizuno, H. Adachi, and I. Tanaka: Phys. Rev. B **61** (2000) 1811.
7) K. Nomura, T. Kamiya, H. Ohta, T. Uruga, M. Hirano, and H. Hosono: Phys. Rev. B **75** (2007) 035212.
8) J. E. Medvedeva: Europhys. Lett. **78** (2007) 57004.
9) T. Kamiya, K. Nomura, M. Hirano, and H. H. V. 5: Phys. Status Solidi C **5** (2008) 3098.
10) T. Kamiya, K. Nomura, and H. Hosono: Phys. Status Solidi A **206** (2009) 860.
11) H. Omura, H. Kumomi, K. Nomura, T. Kamiya, M. Hirano, and H. Hosono: J. Appl. Phys. **105** (2009) 093712.
12) M. D. Segall, P. J. D. Lindan, M. J. Probert, C. J. Pickard, P. J. Hasnip, S. J. Clark, and M. C. Payne: J. Phys.: Condens. Matter **14** (2002) 2717.
13) P. Hohenberg and W. Kohn: Phys. Rev. **136** (1964) B864.
14) W. Kohn and L. J. Sham: Phys. Rev. **140** (1965) A1133.
15) J. P. Perdew, J. A. Chevary, S. H. Vosko, K. A. Jackson, M. R. Pederson, D. J. Singh, and C. Fiolhais: Phys. Rev. B **46** (1992) 6671.
16) D. Vanderbilt: Phys. Rev. B **41** (1990) 7892.
17) G. Kresse and J. Furthmüller: Phys. Rev. B **54** (1996) 11169.
18) R. Car and M. Parrinello: Phys. Rev. Lett. **55** (1985) 2471.
19) B. G. Pfrommer, M. Côté, S. G. Louie, and M. L. Cohen: J. Comput. Phys. **131** (1997) 233.
20) V. G. Tyuterev and N. Vast: Comput. Mater. Sci. **38** (2006) 350.
21) M. Nespolo, A. Sato, T. Osawa, and H. Ohashi: Cryst. Res. Technol. **35** (2000) 151.
22) C.-S. Chuang, T. C. Fung, B. G. Mullins, K. Nomura, T. Kamiya, H.-P. D. Shieh, H. Hosono, and J. Kanicki: SID Int. Symp. Dig. Tech. Pap. **39** (2008) 1215.
23) A. Seidl, A. Görling, P. Vogl, J. A. Majewski, and M. Levy: Phys. Rev. B **53** (1996) 3764.
24) C. Persson, Y.-J. Zhao, S. Lany, and A. Zunger: Phys. Rev. B **72** (2005) 035211.
25) S. Lany and A. Zunger: Phys. Rev. B **78** (2008) 235104.
26) S. J. Clark, J. Robertson, S. Lany, and A. Zunger: Phys. Rev. B **81** (2010) 115311.
27) T. Kamiya, K. Nomura, and H. Hosono: J. Disp. Technol. **5** (2009) 273.
28) H. Hosono: J. Non-Cryst. Solids **352** (2006) 851.
29) A. Janotti and C. G. V. d. Walle: Appl. Phys. Lett. **87** (2005) 122102.
30) T. Kamiya, K. Nomura, and H. Hosono: J. Disp. Technol. **5** (2009) 273.
31) S. Larry and A. Zunger: Phys. Rev. Lett. **98** (2007) 045501.
32) A. Janotti and C. G. V. d. Walle: Nat. Mater. **6** (2007) 44.
33) B. D. Ahn, H. S. Shin, H. J. Kim, J.-S. Park, and J. K. Jeong: Appl. Phys. Lett. **93** (2008) 203506.
34) B. D. Ahn, H. S. Shin, G. H. Kim, J.-S. Park, and H. J. Kim: Jpn. J. Appl. Phys. **48** (2009) 03B019.
35) K. Nomura, A. Takagi, T. Kamiya, H. Ohta, M. Hirano, and H. Hosono: Jpn. J. Appl. Phys. **45** (2006) 4303.
36) B. D. Ahn, H. S. Shin, G. H. Kim, J.-S. Park, and H. J. Kim: Jpn. J. Appl. Phys. **48** (2009) 03B019.
37) M. Nespolo, A. Sato, T. Osawa, and H. Ohashi: Cryst. Res. Technol. **35** (2000) 151.
38) I. Keller and W. Mader: Z. Anorg. Allg. Chem. **636** (2010) 1045.